Lab on a Chip

PAPER

View Article Online
View Journal

Cite this: DOI: 10.1039/d5lc00139k

Scalable and ultrafast CAR-T cell production using microfluidics†

Vladislav Markelov,‡[a] Konstantin V. Arabuli,‡[b] Ivan Gaponenko,[a] Vladislav Sergeev,[a] Alena Shakirova,[a] Kirill V. Lepik,*[a] Alexander D. Kulagin[a] and Mikhail V. Zyuzin*[bc]

Chimeric antigen receptor T cell (CAR-T) therapy has recently gained recognition as a transformative treatment of cancer, particularly of hematological malignancies. However, CAR-T manufacturing remains a major bottleneck of this treatment modality; in standard cases, it takes up to two weeks, resulting in a phenotypic shift toward terminally differentiated T-cells and a significant depletion of T-cells with naive-like phenotype (Tnlp), crucial for sustained clinical efficacy. Leveraging the current progress in microfluidic technologies, we develop and optimize a microfluidic device (MFD) for CAR-T cell production *via* an ultrafast protocol that integrates T-cell activation and lentiviral transduction in a single step within 24 hours. The MFD geometry allowed reaching a transduction rate of 27% (for MOI 3) compared to 17% and 8% transduction (MOI 3) in 48- and 6-well plates, respectively, used as controls. Notably, in the ultrafast protocol in our MFD, the amount of CD3+ Tnlp is approximately six times higher than that remaining after the standard 9 day protocol (18.07 ± 6.03% *vs.* 3.97 ± 2.37%). A similar pattern is noted for CD4+ and CD8+ Tnlp, with percentages of 11.07 ± 6.08% *vs.* 3.56 ± 3.52% and 29.2 ± 7.11% *vs.* 4.18 ± 1.69%, respectively, in the final CAR-T product. Our results highlight MFDs as a scalable platform to streamline CAR-T manufacturing, with the potential to improve clinical accessibility and outcomes by reducing the production time while preserving essential T-cell phenotypes.

Received 10th February 2025,
Accepted 2nd May 2025

DOI: 10.1039/d5lc00139k

rsc.li/loc

Introduction

In recent years, chimeric antigen receptor T-cell (CAR-T) therapy has demonstrated impressive efficacy in a range of hematological malignancies.[1] In particular, anti-CD19 CAR-T became a standard of therapy for refractory and relapsed B-cell leukemia and lymphoma, and anti-BCMA CAR-T, for multiple myeloma.[2,3] Currently, more than 10 commercial and academic CAR-T products for treatment of the above-mentioned diseases have already been approved by national regulatory authorities worldwide. Furthermore, numerous clinical trials are underway, aimed to reveal the applicability of CAR-T for other oncohematological diseases as well as solid cancers and autoimmune pathologies.[4–7]

However, CAR-T therapy has not completely eradicated the problem of refractoriness or relapse in B-cell malignancies. Approximately 50% to 60% of patients treated with anti-CD19 CAR-T do not achieve long-term remissions.[8–11] The reasons for failures are complex and remain an active area of research.[12,13] One recognized challenge is that patients heavily pretreated with chemotherapy or other anticancer therapies often present with T-cell populations that are exhausted and compositionally suboptimal for CAR-T manufacturing, leading to reduced functionality of the final product or, in some cases, manufacturing failure. In addition, current CAR-T manufacturing involves a prolonged *ex vivo* culture step that typically lasts more than 9 days, which leads to phenotype shifting towards more differentiated T-cells.[14,15] Such a lengthy procedure is associated with depletion in the final CAR-T product of the population of naive (Tn) and stem cell memory T-cells (Tscm), which comprise a group of T-cells with a naive-like phenotype (Tnlp). Cells with this phenotype were shown to be essential for sustained antitumor responses due to their high proliferative activity, self-renewing capacity, and ability to differentiate into memory and effector T-cell subsets.[16–18] As a result, CAR-T products depleted of this population are insufficient to achieve durable clinical response. Therefore,

[a] *RM Gorbacheva Research Institute of Pediatric Oncology, Hematology and Transplantation, Pavlov University, 191144 St. Petersburg, Russian Federation. E-mail: lepikkv@gmail.com*
[b] *School of Physics and Engineering, ITMO University, 191002 St. Petersburg, Russia. E-mail: mikhail.zyuzin@metalab.ifmo.ru*
[c] *Moscow Center for Advanced Studies, Kulakova str. 20, Moscow, Russia*
† Electronic supplementary information (ESI) available. See DOI: https://doi.org/10.1039/d5lc00139k
‡ Equal contribution.

development of novel efficient protocols for CAR-T production with a shorter manufacturing time is highly demanded to preserve or enrich scarce Tnlp populations.

Approaches aimed at enriching CAR-T with Tnlp are being actively investigated. Some of them focus on reducing the CAR-T manufacturing time by reducing the *ex vivo* culture period and/or shortening the T-cell activation step up to its complete abolition.[19–21] Other approaches use isolated populations of Tnlp and Tscm to generate CAR-T, or inhibition of differentiation into T-cells with an effector phenotype by pharmacological or other means.[22] However, these protocol modifications should be further tested to reveal their applicability in clinics.

Several research groups have demonstrated *in vitro* and *in vivo* reduction of the CAR-T production step down to ≤3 days, which results in a more robust control of tumor cell proliferation.[15,19] The first results of clinical trials of this shortened CAR-T protocol demonstrated an increased efficacy and a lower incidence of adverse events associated with immunotherapy.[23–25]

Next-day CAR-T approaches were reported, with "ultrafast" manufacturing taking less than 24 h,[20] employing non-activated T-cells or T-cells under conditions of simultaneous activation and transduction. However, these protocols are hampered by the inherently low efficiency of transduction by viral vectors, particularly lentiviral vectors (LVs).[19,21] This inefficiency requires the use of high viral titers, which substantially increases the production costs, as LV particles remain one of the most expensive components for CAR-T manufacturing.[26–28]

To overcome the obstacles mentioned, the transduction efficiency of T-cells can be improved using advantageous conditions. For instance, applying the modified geometry of a culture plate or microfluidic device can enhance the interaction of LV with cells.[29] For instance, Sin *et al.* reported the development of a microfluidic bioreactor designed for the non-simultaneous activation and transduction of T-cells with the capability for continuous medium perfusion by compensating for evaporation and maintaining pH (7.4) and temperature (37 °C) in order to enhance transduction efficiency.[30] As a result, the protocol achieved a tenfold higher cell density compared to gas-permeable plates, provided metabolic control through online monitoring of O_2, pH, glucose, and lactate, and reduced production time to 12 days compared to the 14–21 days required by standard protocols—significantly improving the efficiency of CAR-T cell manufacturing and making the therapy more accessible and standardized. In another study, Tran *et al.* reported that traditional methods are ineffective due to limitations in the mass transfer of viral particles to cells. Microfluidic systems can reduce diffusion distances and increase the local concentration of virus particles around cells.[29] This optimization leads to higher transduction efficiency using less LV. Nonetheless, the potential for shortening the protocol through simultaneous activation and transduction of T-cells within the microfluidic device has not yet been investigated. In this regard, we develop and optimize a microfluidic platform for ultrafast CAR-T production. By leveraging the advantages of microfluidic technologies, we aim to improve the efficiency of T-cell transduction by LV under conditions of simultaneous activation and transduction and reduce the manufacturing time down to 24 h, both improving the yield of CAR-T cells and enriching the final product with Tnlp.

Methods

Fabrication of the microfluidic device (MFD)

Polydimethylsiloxane (PDMS) was used to fabricate microfluidic devices by a "soft" lithography technique using a mold obtained with 3D printer technologies. A detailed description of the microfluidic device fabrication route is presented in the ESI.†

Selection and activation of T-cells

All experiments in this study abide by applicable national and international regulations and guidelines and approved by the First Pavlov State Medical University of St. Petersburg institutional scientific review board. The study is in line with data protection and privacy regulations. All patients signed informed consent. Apheresis samples were collected from healthy donors in accordance with the Helsinki declaration. Peripheral blood mononuclear cells (PBMCs) were obtained by separation in Ficoll density gradient using SepMate tubes (STEMCELL Technologies, Canada). For separation of T-cells after isolation, PBMCs were incubated with anti-TCRα/β antibodies conjugated to biotin, followed by incubation with anti-biotin antibodies (Miltenyi Biotec, Germany) or anti-CD4/CD8 nanobeads (GenScript Biotech, USA). Next, magnetic selection of T-lymphocytes was performed using MACS Columns (Miltenyi Biotec, Germany) in accordance with the manufacturer's protocol.

After the selection, the T-cells were placed into the wells of a non-treated culture plate in X-VIVO 15 medium (Lonza, Switzerland) supplemented with 5% human serum (HiMedia, India), IL-7 (BioLegend, USA), and IL-15 (BioLegend, USA), the last two at a concentration of 10 ng ml^{-1}. For activation, biodegradable nanoparticles coated with anti-CD3 and anti-CD28 antibodies (Enceed™, GenScript Biotech, USA) were added to the cell suspension; after that, the T-cells were incubated for 48 h at a temperature of 37 °C with a CO_2 concentration in air of 5%.

CAR-T manufacturing and optimization of T-cell transduction in an MFD

For the initial optimization of MFD CAR-T manufacturing, 0.2×10^6 of the activated T-cells were washed and resuspended in X-VIVO 15 medium (Lonza, Switzerland) supplemented with 5% inactivated human serum (HiMedia, India), IL-7 (BioLegend, USA), IL-15 (BioLegend, USA), and

protamine sulfate (Ellara, Russia) at a concentration of 10 μg ml^{-1}. Then, the T-cells were mixed with third-generation lentiviral vector particles pseudotyped with vesicular stomatitis virus glycoprotein (VSV-G). The LV particles carried a transgene encoding an anti-CD19 chimeric antigen receptor (CAR), comprising the FMC63 antigen-binding domain and signaling domains from 4-1BB and CD3ζ. CAR-coding LV particles were added to cells at various multiplicities of infection (MOI = 1, 3, 5, and 30) and subsequently placed in a microfluidic device (MFD) for 6–24 h. Depending on the chip channel height (50 μm, 100 μm, 150 μm, or 200 μm), the final suspension volume was calculated to be 8.3 μl, 16.6 μl, 25 μl, and 33 μl, respectively. After incubation in an MFD, T-cells were transferred to a 48-well plate, where the suspension volume was increased 5-fold with a medium without protamine sulfate. As a control, 1.0×10^6 activated T-cells were washed and resuspended in 200 μl of the same medium at a final concentration of 5.0×10^6 T-cells per 1 ml. Afterwards, the control T-cell suspension was placed in a 48-well plate and spinoculated at 600*g* for 40 min. Then, the cells were transferred to a 12-well plate with the medium without protamine sulfate, with the final volume increased 5-fold. After that, the plate was placed in an incubator for 24 h.

After 24 h of transduction, the medium was replaced with fresh X-VIVO 15 medium with 5% human serum, IL-7, and IL-15. The starting day of transduction was considered day 0. Transduction efficiency was assessed on day 7 using flow cytometry.

Concurrent T-cell activation and transduction in an MFD

Then, we assessed the capability of our MFDs to provide the transduction of T-cells under conditions of one-step activation and transduction (concurrent activation and transduction of T-cells in an MFD/well plate). For this, 1.8×10^6 T-cells were placed in an MFD with an increased incubation area and a channel height of 150 μm. After magnetic selection, T-cells were mixed with X-VIVO 15 medium supplemented with 5% inactivated human serum, IL-7, IL-15, protamine sulfate at a concentration of 10 μg ml^{-1}, biodegradable nanoparticles for activation, and LV at MOI 3, and placed in the MFD for 24 h. The final volume of the suspension loaded into the MFD was 110 μl. Here, two controls were used: for control 1, 1.8×10^6 T-cells were transduced in a 48-well plate at a final volume of 110 μl for 24 h. For control 2, T-cells were incubated in a 6-well plate at a final volume of 1.8 ml for 24 h. Afterwards, the medium was replaced with a fresh one without protamine sulfate, and the T-cells were transferred to a 12-well culture plate. As before, the start of transduction was considered day 0. Transduction efficiency was assessed on day 7 using flow cytometry. Cell counts were performed using a light microscope and trypan blue.

CAR-T production using standard, fast and ultrafast protocols

Next, we compared the subpopulation composition of the CAR-T cells manufactured using different protocols. For the next-day (ultrafast) manufacturing protocol, T-cells were mixed with LV (MOI 3) and biodegradable nanoparticles for activation, and then placed in a 110 μl MFD for 24 h. For the ultrafast control, the same volume of mixture of T-cells with biodegradable particles for activation and LV (MOI 3) was placed in a 48-well plate for 24 h. In the fast (72 h) and standard (9 days) protocols, isolated T cells were first activated for 48 h, and then, these activated T-cells were transferred to a 48-well plate containing LV (MOI 3) for 24 h for static transduction. Immunophenotypic characteristics of the obtained CAR-T were assessed at the end of the manufacturing protocol: on day 1 for the ultrafast protocol, on day 3 for the fast protocol, and on day 9 for the standard protocol. Due to the phenomenon of pseudo transduction, the level of true transduction for each protocol was assessed at day 9.

Flow cytometry

The phenotypes of the initial T-cells and the obtained CAR-T were characterized using flow cytometry with the following staining: anti-CD3-FITC (Elabscience, clone UCHT1), anti-CD45RO-APC (BioLegend, clone UCHL1), anti-CCR7-PE/Cyanine7 (BioLegend, clone G043H7), anti-CD8-Elab Fluor Violet 450 (Elabscience, clone OKT-8), and anti-CD4-PerCP/Cyanine5.5 (BioLegend, clone OKT-4). The level of T-cell transduction was measured using anti-FMC63-PE (ACROBiosystems, cat. no. FM3-PY54G0). T-cells were incubated with anti-FMC63 antibodies for 30 min at 4 °C, and then the remaining antibodies were added and incubated for 30 min at 4 °C. After the cells were washed twice in 2 ml of PBS for 5 min at 350*g*, the cells were incubated with LIVE/DEAD Draq7 (BioLegend) for 15 min. Flow cytometry was performed using a BD FACSCanto II system (BD Biosciences). Data were processed using Kaluza Analysis Software (Beckman Coulter). Based on the expression of CD45RO and CCR7 among CD3+FMC63±CD4+ and CD3+FMC63±CD8+, the following phenotypes were identified: CD45RO−/CCR7+, Tnlp; CD45RO+/CCR7+, central memory T-cells (Tcm); CD45RO+/CCR7−, effector memory T-cells (Tem); and CD45RO−/CCR7−, terminal differentiated T-cells (Temra). The gating strategy is presented in the ESI.†

Statistical analysis

Data are presented as mean values with standard deviation. For intergroup analysis, the nonparametric Kruskal–Wallis test was used. For pairwise analysis, the nonparametric Mann–Whitney test was used. Statistical analysis and data visualization were performed using R software version 4.2.1, GraphPad Prism 10.1.1 and OriginLab version 10.100173. Illustrations were created using BioRender Software.

Results and discussion

Optimization of an MFD

Microfluidic devices were fabricated using a soft lithography procedure as described elsewhere[31] (Fig. S1†). Two geometries of microfluidic devices were considered: (i) snake-like geometry and (ii) increased incubation area geometry (Fig. S2†).

The topologies used in this work were structurally identical: both had one input for injecting a mixture of LV and T-cells, the incubation area, and one output. The main difference between the topologies is the incubation area, which is 1.66 cm^2 for the snake-like geometry and 10 cm^2 for the increased incubation area geometry. To reveal how the geometric parameters affect the transduction efficiency, we varied the height of the microfluidic channel, the incubation time, and the amount of virus per T-cell (multiplicity of infection, MOI) (Fig. 1). As the channel height decreases, the total incubation volume of LV with activated T-cells changes accordingly, reducing the "free path" between LV and activated T-cells; however, it creates the risk of decreasing the viability of T-cells due to limited nutrient exchange. The heights used were 50, 100, 150, and 200 μm (Fig. S3†), which correspond to 8.3, 16.6, 25, and 33 μl. After introduction of LV mixed with activated T-cells at MOI 30, the MFD was placed in an incubator for 6 h. Then, the transduced cells were collected from the MFD and analyzed using flow cytometry for the assessment of cell viability and CAR expression. According to the obtained data, heights of the MFD channel did not affect the T-cells' viability, which exceeded 90% for all the heights tested. Also differences in the transduction efficiency of activated T-cells by the LV were not registered for different channel heights of the MFD. For instance, the transduction was 47% for the 50 μm channel height, 41% for 100 μm, 42% for 150 μm, and 43.13% for 200 μm (Fig. S4†). The absence of significant differences in the transduction efficiency can be explained by the increased amount of added LV (MOI 30). In the MFD geometry used, reducing the channel height to 50 μm decreased the working volume to 8.3 μL, introducing technical challenges associated with handling such small volumes. This reduction resulted in increased instrumental error during experiments. To mitigate these issues, we selected a channel height of 150 μm for subsequent experiments, corresponding to a working volume of 25 μL and a reduced MOI of 3.

Further, we investigated the influence of incubation duration (with 6, 12, 18, and 24 h time frames) on the transduction efficiency of T-cells at a fixed MOI of 3 in the MFD. During the first day of incubation in each MFD, the number of CAR-expressing T-cells increased gradually with incubation time. For instance, this number was 31 ± 11% after 6 h, 41 ± 18% after 12 h, 50 ± 15% after 18 h, and 69 ± 16% after 24 h. Notably, on the 7th day of culturing, the number of CAR-expressing T-cells significantly decreased and was equal to 10 ± 3% after 6 h, 13 ± 4% after 12 h, 20 ± 2% after 18 h, and 15 ± 5% after 24 h (Fig. 2B and C). This

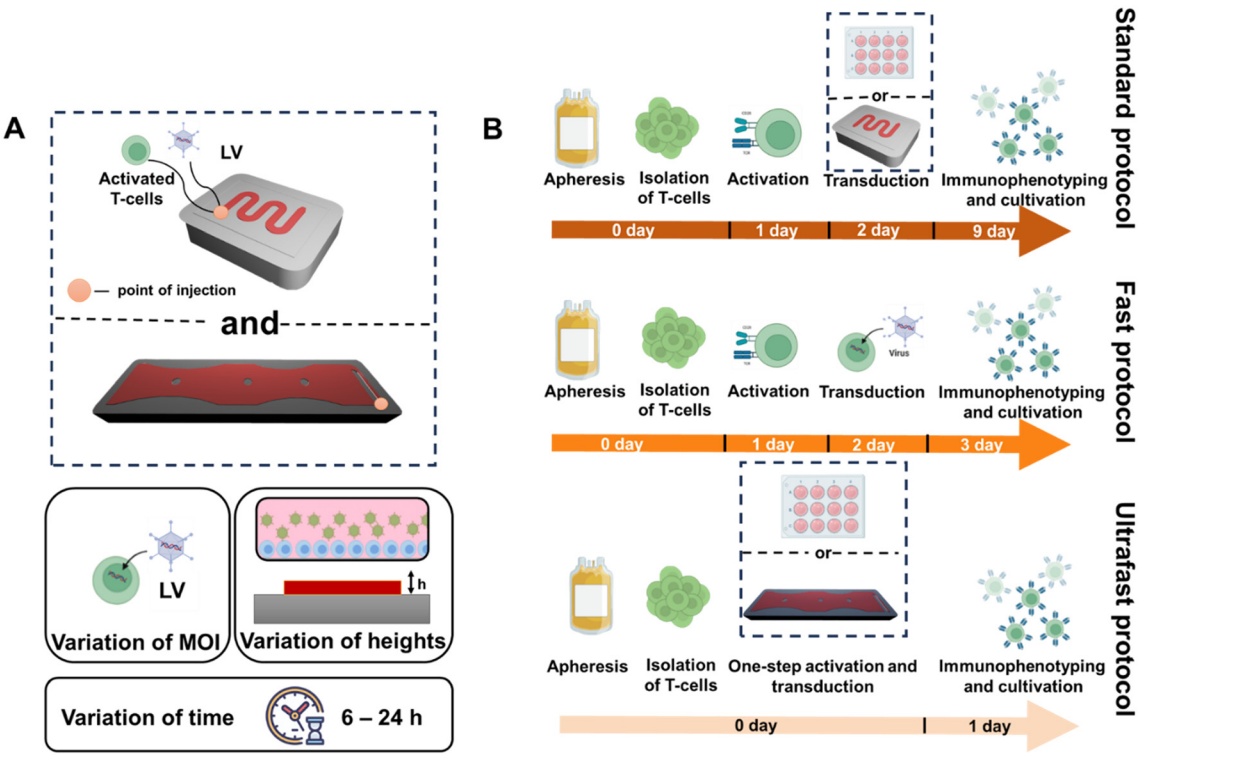

Fig. 1 (A) Schematic illustration of the used MFD and performed optimization steps, which include variation of MOI, channel heights, and incubation time. (B) Schematic illustration of ultrafast, fast, and standard protocols.

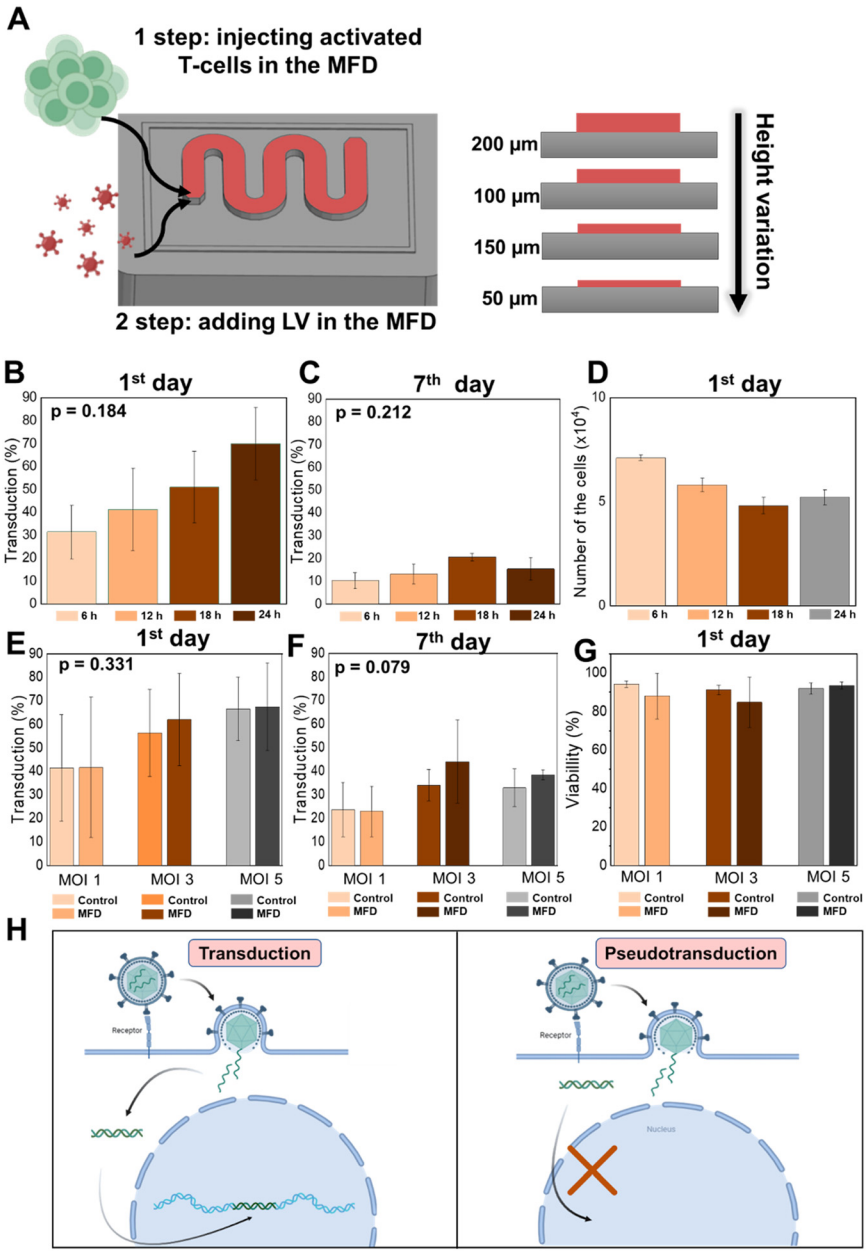

Fig. 2 Optimization of CAR T-cell production using MFD. (A) Schematic illustration of CAR T-cell production in our MFD. (B) Transduction efficiency of T-cells at fixed MOI 3 on the 1st day (6, 12, 18, 24 h time points) in an MFD. (C) Transduction efficiency of T-cells at fixed MOI 3 on the 7th day (6, 12, 18, 24 h time points) in an MFD. D. T-cells yield on the 1st day (6, 12, 18, 24 h time points) in an MFD. E. Transduction efficiency of T-cells at different MOIs (1, 3, 5) on the 1st day (6, 12, 18, 24 h time points) in an MFD. F. Transduction efficiency of T-cells at different MOIs (1, 3, 5) on the 7th day (6, 12, 18, 24 h time points) in an MFD. G. T-cell viability at different MOIs (1, 3, 5) on the 1st day (6, 12, 18, 24 h time points) in an MFD. H. Schematic illustration of the transduction and pseudotransduction processes.

lowered transduction efficiency can be explained by the so-called pseudotransduction caused by the temporary expression of CAR on the surface of T-cells without the integration of the transgene into the genomic DNA (Fig. 2H). The reason for this is the fusion of the supercapsid of the LV, carrying CAR on its surface, with the membrane of the T-cell, which makes the latter transiently CAR-positive. Additionally, the T-cell yield was similar and equal to $7.1 \times 10^4 \pm 0.13$ cells after 6 h of incubation, $5.8 \times 10^4 \pm 0.32$ cells after 12 h, $4.8 \times 10^4 \pm 0.39$ cells after 18 h, and $5.2 \times 10^4 \pm 0.37$ cells after 24 h (Fig. 2D). Therefore, the 24 h incubation was used for further MFD experiments.

To reveal how MOI impacts the production of CAR T-cells in an MFD, we varied the amount of virus particles per cell (MOI 1, 3 and 5). Notably, for the control, we used a manufacturing protocol that included both spinoculation (600*g* for 40 min) and a static transduction step in a well plate. According to the obtained data, increasing the number of transducing units of the viral vector increases the transduction efficiency. However, after a certain threshold, a

further increase in the number of MOI is not accompanied by a further increase in the level of transduction (Fig. 2E and F). For instance, the transduction efficiency on the 1st day for MOI 1 was 42 ± 30%, for MOI 3, 62 ± 19%, and for MOI 5, 67 ± 18% (p = 0.331). Consequently, the transduction efficiency on the 7th day for MOI 1 was equal to 23 ± 10%, for MOI 3, to 44% ± 18, and for MOI 5, to 38 ± 2% (p = 0.079). Pairwise analysis of transduction results obtained in the MFD and in the control at different MOI on day 1 and day 7 revealed no significant differences for both cases. The proportion of viable T-cells after 24 h of transduction in the MFD and in the control was also similar and equal to 94 ± 1.7% (control) and 88 ± 12% (MFD) for MOI 1, 91 ± 2% (control) and 84 ± 13% (MFD) for MOI 3, and 91 ± 2.8% (control) and 93 ± 1.8% (MFD) for MOI 5 (Fig. 2G).

The plateau reached when we varied the MOI level indicates that there is an optimal range for MOI, and beyond it, additional viral vectors do not enhance the transduction efficiency.[32] Importantly, for all the used MOI levels, the T-cell viability remained high (>85%). The transduction rates were comparable to those achieved with optimized protocols with spinoculation, which enhances the efficiency but complicates clinical-scale production. The use of MFDs with modified geometric conditions and a similar MOI allowed us to achieve transduction results comparable to those of the control, eliminating the need for an additional spinoculation stage in the manufacturing process. These findings confirm the applicability and effectiveness of our MFD approach for streamlined CAR-T cell production.

Immunophenotyping of T-cells after transduction in an MFD

To reveal how our MFD affects the phenotype of T-cells after the transduction, we analyzed the effect of the MFD incubation duration on the T-cell subpopulations and their dynamics during subsequent cultivation using flow

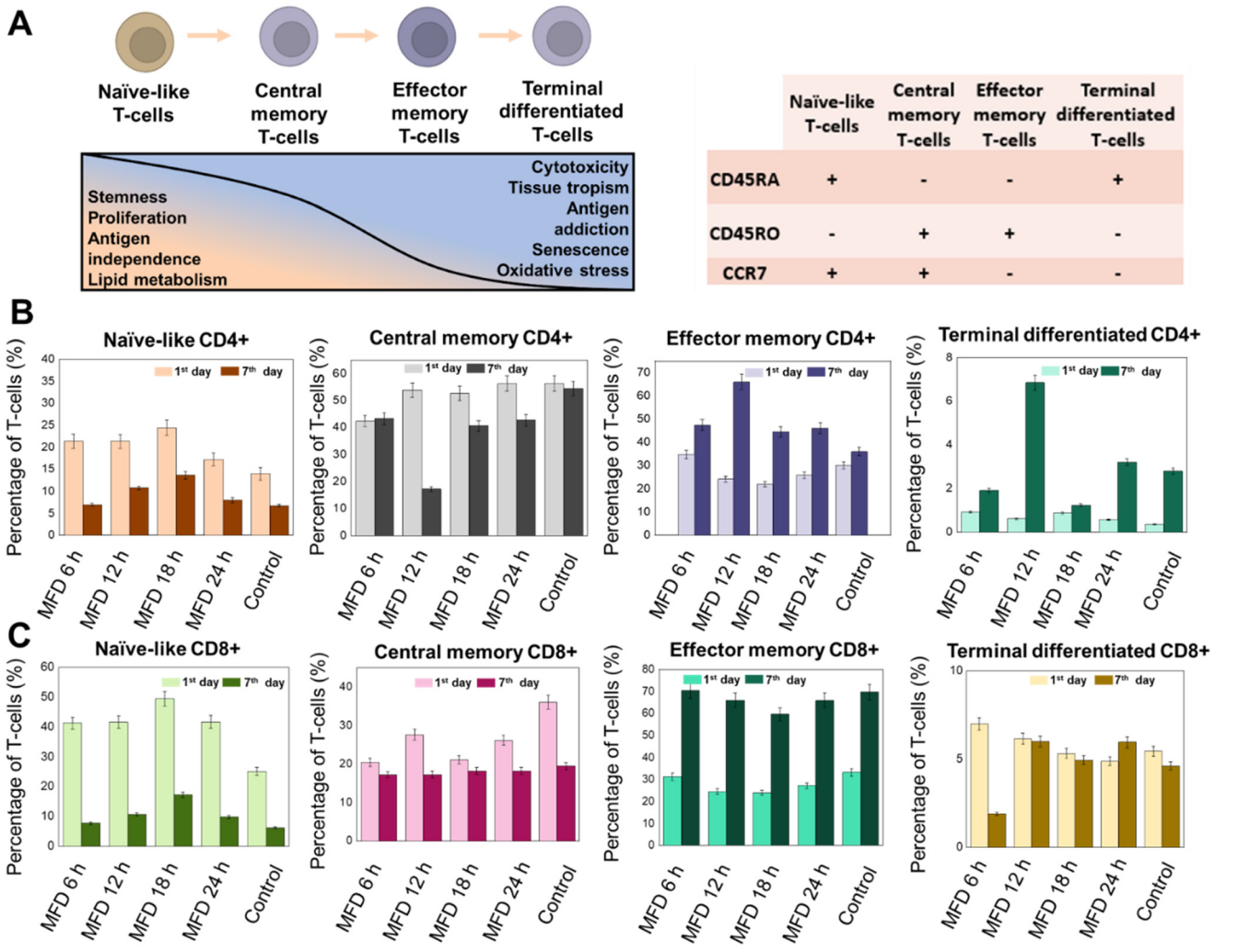

Fig. 3 Immunophenotyping of T-cells after transduction. (A) Schematic illustration of the evolution of T lymphocytes and their properties. (B) Percentage of CD4+ T-lymphocytes according to their subpopulation composition on the 1st and 7th days (6, 12, 18, 24 h time points) after transduction in an MFD. (C) Percentage of CD8+ T-lymphocytes according to their subpopulation composition on the 1st and 7th days (6, 12, 18, 24 h time points) after transduction in an MFD.

cytometry. As a control, transduction in a standard well plate was performed (Fig. 3A). The following subpopulations of CD4+ and CD8+ T-cells were assessed: naive-like T cells (Tnlp), central memory T cells (Tcm), effector memory T cells (Tem), and terminally differentiated effector T cells (Temra) on the 1st and 7th days post-transduction (Fig. 3B and C). Overall, fractions of Tnlp, Tcm, Tem and Temra on days 1 and 7 were comparable for the groups incubated for 6, 12, 18, or 24 h in the MFD and those transduced in a well plate.

Flow cytometry results (Fig. 3B) indicated the tendency for higher Tnlp in the MFD compared to the control. The number of Tnlp CD4+ is considerably higher after culture initiation on day 1 than on day 7. This decrease is attributed to the activation-induced differentiation of Tnlp into Tcm, Tem, and Temra subpopulations. These changes are a result of activation signals, which drive the maturation of Tnlp into more specialized subsets, contributing to the observed reduction in Tnlp by day 7. For the Tnlp CD8+ (Fig. 3C), we also notice a decrease in the fraction of Tnlp on day 7 due to the processes described above.

Concurrent T-cell activation and transduction in an MFD

To evaluate the efficiency of transduction in our MFD using concurrent activation and transduction of T-cells, we incubated 1.8×10^6 T-cells with LV and biodegradable nanoparticles for activation in the MFD for 1 day. For this, we used the MFD with an increased incubation area topology and 150 μm channel height (Fig. 4A and B). Here, two controls for the CAR-T production were considered. For control 1, we used a standard well of a 48-well plate, in which LV, activating biodegradable nanoparticles, and 1.8×10^6 T-cells were mixed to a volume of 110 μL and incubated for 24 h. In turn, control 2 was performed in a 6-well plate, where the same amount of LV, activating biodegradable nanoparticles, and T-cells was added and diluted up to 1.8 mL.

As previously, transduction efficiency was assessed using flow cytometry. The 7th day was chosen to assess the level of transduction because up to that time, we had observed the effects of pseudotransduction (Fig. S8†). According to the obtained data, the transduction level on the 7th day at MOI 3 was 27 ± 8% using MFD, 17 ± 8% in control 1, and 8 ± 6% in control 2 (Fig. 4C). Analysis of the transduction data indicates a trend toward higher efficiency in the MFD compared to control 1 ($p = 0.100$) and a statistically significant improvement compared to control 2 ($p = 0.040$) (Fig. 4C). Increased CAR-T production in the MFD can be attributed to the optimized geometrical parameters, *i.e.*, decreased "free path length" between T-cells and LV. Additionally, kinetics of T-cell proliferation was similar for MFD and both controls (Fig. 4D). Thus, it can be concluded that simultaneous activation and transduction under MFD conditions increases the transduction efficiency of T-cells and does not affect their further proliferative potential. The transduction efficiency of 27% for T-cells is relatively high,[21] considering that cells did not initially undergo the activation process. This result demonstrates the success of the optimized transduction methodology and can serve as a reliable basis for further ultrafast protocols.

CAR-T production using ultrafast protocol in an MFD

Further, to investigate the immunophenotype of the CAR-T product manufactured in an MFD and in well plates

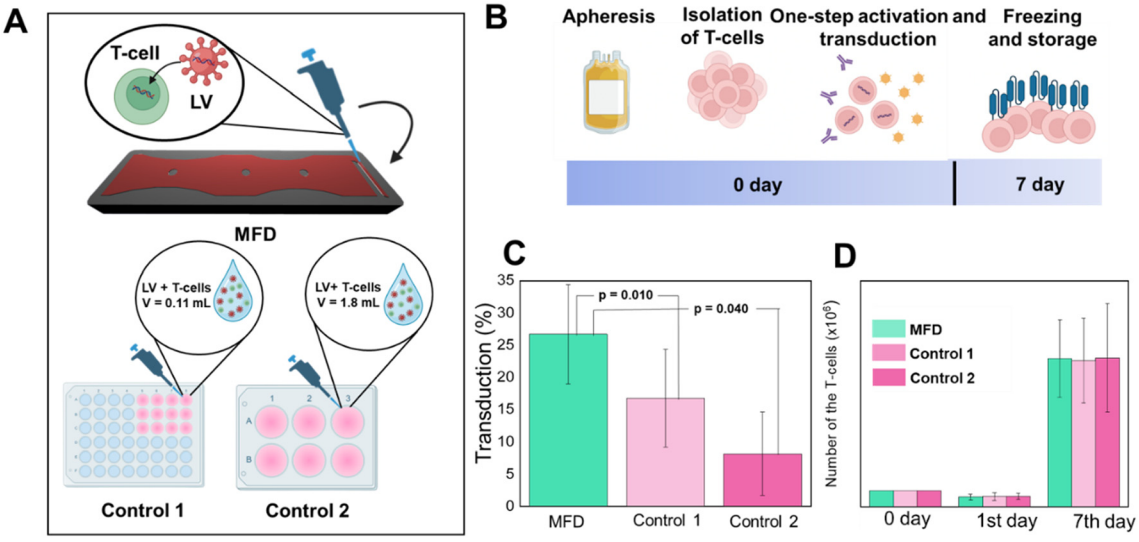

Fig. 4 Concurrent T-cell activation and transduction in an MFD. (A) Schematic illustration of the experimental procedure in an MFD and controls that were used. (B) Schematic illustration of the protocol duration, which includes apheresis, isolation of T-cells, one-step activation and transduction and proliferation. (C) Transduction efficiency of T-cells incubated in an MFD and in well plates (control 1 and control 2) on day 7. (D) Proliferation efficiency of T-cells incubated in an MFD and in well plates (control 1 and control 2) on days 0, 1, and 7.

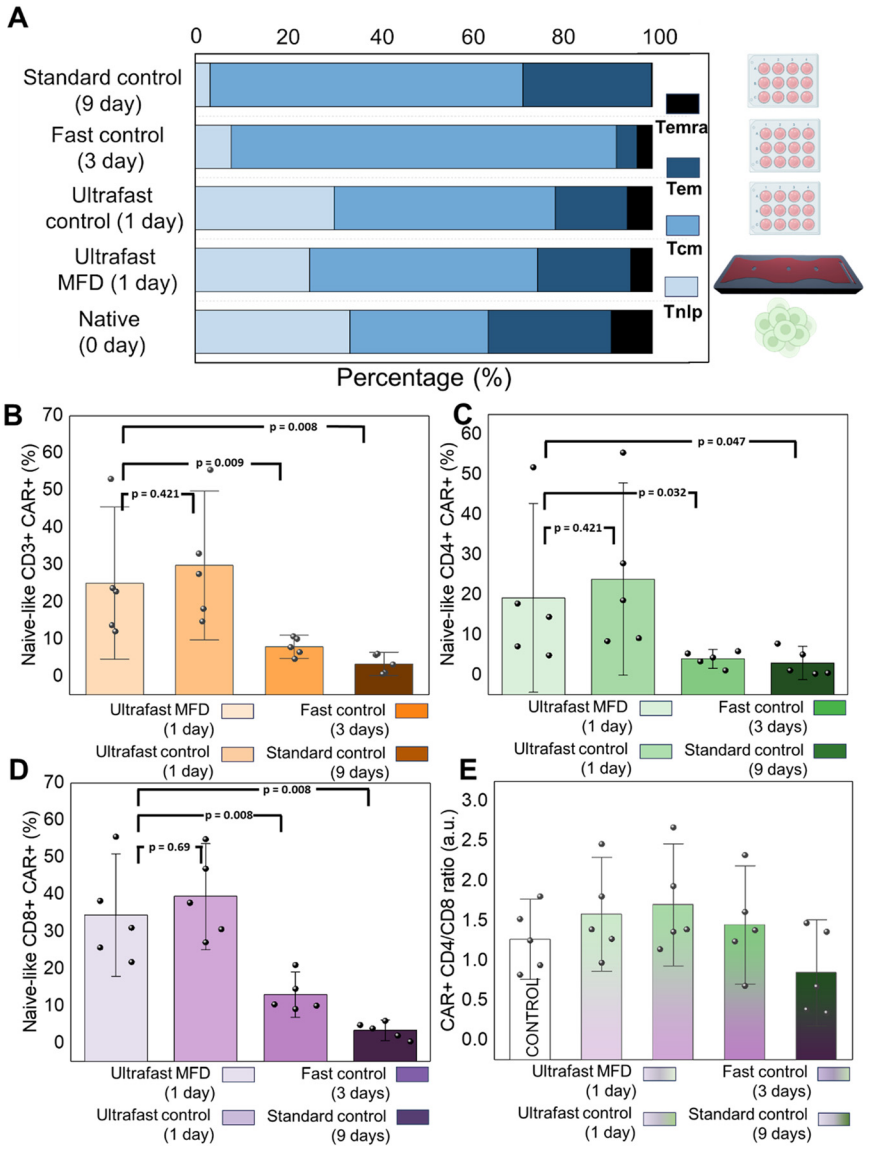

Fig. 5 CAR-T production using standard, fast, and ultrafast protocols. (A) Immunophenotype of CAR-T cells according to the used protocol. (B) Percentage of naive-like CD3+ CAR-expressing cells. (C) Percentage of naive-like CD4+ CAR-expressing cells. (D) Percentage of naive-like CD8+ CAR-expressing cells. (E) Ratio of CD4+/CD8+ CAR-expressing cells.

(control), we used three protocols: standard, fast, and ultrafast (Fig. 5A). In the ultrafast protocol, activation and transduction were performed concurrently in MFDs within 24 h. In contrast, the fast and standard protocols involved sequential steps: T-cells were first activated, and lentiviral transduction followed. The only difference between fast and standard protocols is the overall duration, which was 3 days for fast and 9 days for standard. Additionally, we analyzed native T-cells directly after immunomagnetic selection that were neither activated nor transduced by LV.

We analyzed subpopulations CD3+, CD4+, and CD8+ of Tnlp obtained in the three protocols. The amount of Tnlp obtained in the ultrafast MFD protocol was comparable to the values in the ultrafast control for both CD3+ (25.05 ± 16.47% *vs.* 29.75 ± 16.09%; $p = 0.421$), CD4+ (19.21 ± 18.95% *vs.* 23.88 ± 19.33%; $p = 0.421$), and CD8+ (34.46 ± 13.28% *vs.* 39.45 ± 11.45%; $p = 0.690$). Compared to the ultrafast MFD, the amount of CD3+ Tnlp obtained using fast control and standard control protocols was lower (7.93 ± 2.49% ($p = 0.009$) and 3.29 ± 2.55% ($p = 0.008$), respectively). Also, separately for CD4+ and CD8+ CAR-T subpopulations, a decrease in the proportion of Tnlp was observed with longer manufacturing protocols. For CD4+ CAR-T with nlp, the proportion of this population was 4.01 ± 1.89% ($p = 0.032$) in the fast protocol and 2.94 ± 3.35% ($p = 0.047$) in the standard protocol. For CD8+ CAR-T with nlp it was 13.04% ± 4.92 ($p = 0.008$) in the fast protocol and 3.42% ± 2.23 ($p = 0.008$) in the standard protocol (Fig. 5B–D).

The data demonstrated that the ultrafast protocol preserved a higher proportion of Tnlp cells compared to the

other manufacturing protocols. Native T cells contained 32% Tnlp cells. In the ultrafast MFD and ultrafast control protocols, this population was preserved at 18% and 23%, respectively. In contrast, in the fast control protocol, only 8% Tnlp cells remained, and the standard control protocol showed a further reduction to 4%. The main subpopulation in all the manufacturing protocols was CAR-T with central memory phenotype. They were represented to the greatest extent in the fast protocol. Moreover, in the 9 day standard protocol, an increase in the percentage of differentiated CAR-T effector memory cells was observed. The ultrafast CAR-T manufacturing protocol avoids prolonged *ex vivo* culture of T cells (7 days or more) to preserve the naive-like T-cell phenotype, which is critical for therapeutic efficacy. In our experiments, only a subset of cells was cultured longer to assess transduction efficiency *via* flow cytometry, while the majority were cryopreserved for future use. Extending the culture period to 9 days post-transduction would have resulted in the ultrafast group exhibiting a phenotype similar to that of the standard protocol due to the natural differentiation of T cells during extended cultivation.

During CAR-T manufacturing, in the course of cultivation of T-cells, a natural process of their differentiation occurs. Thus, the population with high proliferative potential and stemness properties, namely, Tnlp, differentiates towards cells with a high cytotoxic potential and limited proliferative activity, Tem and Temra. Accordingly, a longer *ex vivo* cultivation stage leads to the final product more depleted of Tnlp and enriched with Tem and Temra. Generally, preserving nlp in CAR-T is essential, as demonstrated by clinical studies of recent years,[33] where the number of these cells in the final product was directly related to the survival rates of patients with aggressive B-cell lymphomas. Recent data also confirm that CAR-T cells with a preserved Tnlp subpopulation have improved antitumor and repopulation activity compared to CAR-T with a more differentiated phenotype, especially in tests using low doses of CAR-T. There are various approaches to limit T-cell differentiation during the CAR-T production process. One of these is reducing the *ex vivo* duration of cultivation, as shown in our study. As a result of the limited duration due to the freezing step, the cascade of differentiation events is not fully achieved. Here we demonstrate that only 72 h after the start of activation, the CAR+ Tnlp level significantly decreases, while the ultrafast protocol lasting 24 h preserves Tnlp in the final product.

The ratio of CD4+ to CD8+ CAR-T in the product is another variable that may influence the efficacy and toxicity of treatment. The predominance of CD4+ CAR-T is often considered a factor associated with better patient outcomes.[34,35] However, a direct cause-and-effect relationship has not been proven. Based on the obtained data, the CD4+/CD8+ ratio in the initial samples (control) was 1.20 ± 0.44. While statistical analysis did not show a significant difference in the CD4+/CD8+ ratio between the protocols (p = 0.124), a trend was observed: the ultrafast MFD (1.63 ± 0.65), ultrafast control (1.78 ± 0.68), and fast (1.50 ± 0.68) protocols maintained higher CD4+/CD8+ ratios compared to the standard protocol (0.69 ± 0.47) (Fig. 5E). According to the conditions used in this study, a predominant expansion of CD8+ CAR-T was observed. However, in the ultrafast and fast protocols, CD4+ CAR-T cells still remained quantitatively dominant.

Conclusion

We report on the development and optimization of a microfluidic platform for the production of CAR-T cells. By leveraging the advantages of microfluidics, we introduce a novel ultrafast manufacturing process that significantly reduces the *ex vivo* culture period to 24 h, maintaining a higher fraction of CAR+ Tnlp (naive-like T-cells). In the case of the ultrafast protocol obtained in an MFD, the amount of CD3+ Tnlp was approximately 6 times higher compared to the standard protocol, which lasted 9 days (18.07 ± 6.03% *versus* 3.97 ± 2.37%). The same trend was observed in the case of CD4+ and CD8+ Tnlp for ultrafast and standard protocols (11.07 ± 6.08% *versus* 3.56 ± 3.52% and 29.2 ± 7.11% *versus* 4.18 ± 1.69%, respectively) in the final CAR-T product. This approach highlights the importance of optimizing manufacturing processes to enhance clinical outcomes. The functional activity of CAR-T cells produced using the ultrafast MFD protocol was validated through experiments involving multiple biological replicates. Furthermore, the antitumor potential and proliferative capacity of CAR-T cells generated by the ultrafast protocol were further evaluated (Fig. S6†). However, a direct comparison of the anticancer activity of CAR-T cells generated using the ultrafast, fast, and standard protocols is not feasible due to ongoing transgene integration and phenotypic maturation in the ultrafast protocol group. To enable accurate comparisons, the inclusion of an additional pre-cultivation step for CAR-T cells produced by the ultrafast protocol would be advantageous; however, this step was not incorporated into the experimental design of the present study.

Concurrent T-cell activation and transduction within an MFD using the ultrafast protocol also increased the transduction rates. For instance, in our MFD, the transduction level on the 7th day for MOI 3 was 27 ± 8%, whereas in a 48-well plate, this parameter reached 17 ± 8%, and in a 6-well-plate, 8 ± 6%. This has led to significant advances in CAR-T production, particularly in terms of preserving the T-cell subpopulations with high proliferation potential and stemness properties. Specifically, we have demonstrated that prolonged cultivation *ex vivo* depletes T-cells of the Tnlp population and enriches them with more differentiated T-cells (Tem and Temra). This can negatively affect the efficacy of CAR-T therapy. In contrast, decreased *ex vivo* cultivation duration can effectively preserve Tnlp, which correlates with improved survival and increased antitumor activity.

Thus, the use of the MFD as a platform for CAR-T production opens up prospects for the creation of new manufacturing protocols and a reduction in their costs, which could improve the accessibility and effectiveness of this method for treating cancer and other diseases.

Data availability

The data supporting this article have been included as part of the ESI.†

Conflicts of interest

There are no conflicts to declare.

Acknowledgements

Part of this work related to the fabrication of microfluidic devices was supported by the Russian Science Foundation (25-73-20100). The authors also acknowledge the Priority 2030 Federal Academic Leadership Program.

References

1 K. M. Cappell and J. N. Kochenderfer, *Nat. Rev. Clin. Oncol.*, 2023, **20**, 359–371.
2 J. A. Snowden, I. Sánchez-Ortega, S. Corbacioglu, G. W. Basak, C. Chabannon, R. de la Camara, H. Dolstra, R. F. Duarte, B. Glass, R. Greco, A. C. Lankester, M. Mohty, B. Neven, R. P. de Latour, P. Pedrazzoli, Z. Peric, I. Yakoub-Agha, A. Sureda, N. Kröger and European Society for Blood and Marrow Transplantation (EBMT), *Bone Marrow Transplant.*, 2022, **57**, 1217–1239.
3 A. S. Kanate, N. Majhail, Z. DeFilipp, B. Dhakal, B. Dholaria, B. Hamilton, A. F. Herrera, Y. Inamoto, T. Jain, M.-A. Perales, P. A. Carpenter and M. Hamadani, *Transplant. Cell. Ther.*, 2023, **29**, 594–597.
4 A. Daei Sorkhabi, L. Mohamed Khosroshahi, A. Sarkesh, A. Mardi, A. Aghebati-Maleki, L. Aghebati-Maleki and B. Baradaran, *Front. Immunol.*, 2023, **20**(14), 1113882.
5 F. Müller, J. Taubmann, L. Bucci, A. Wilhelm, C. Bergmann, S. Völkl, M. Aigner, T. Rothe, I. Minopoulou, C. Tur, J. Knitza, S. Kharboutli, S. Kretschmann, I. Vasova, S. Spoerl, H. Reimann, L. Munoz, R. G. Gerlach, S. Schäfer, R. Grieshaber-Bouyer, A.-S. Korganow, D. Farge-Bancel, D. Mougiakakos, A. Bozec, T. Winkler, G. Krönke, A. Mackensen and G. Schett, *N. Engl. J. Med.*, 2024, **390**, 687–700.
6 X. Lyu, L. Gupta, E. Tholouli and H. Chinoy, *Rheumatology*, 2024, **63**, 1206–1216.
7 C. Gao, X. Li, Y. Xu, T. Zhang, H. Zhu and D. Yao, *J. Cell. Mol. Med.*, 2024, **28**, e18369.
8 S. J. Schuster, C. S. Tam, P. Borchmann, N. Worel, J. P. McGuirk, H. Holte, E. K. Waller, S. Jaglowski, M. R. Bishop, L. E. Damon, S. R. Foley, J. R. Westin, I. Fleury, P. J. Ho, S. Mielke, T. Teshima, M. Janakiram, J.-M. Hsu, K. Izutsu, M. J. Kersten, M. Ghosh, N. Wagner-Johnston, K. Kato, P. Corradini, M. Martinez-Prieto, X. Han, R. Tiwari, G. Salles and R. T. Maziarz, *Lancet Oncol.*, 2021, **22**, 1403–1415.
9 J. S. Abramson, M. L. Palomba, L. I. Gordon, M. Lunning, M. Wang, J. Arnason, E. Purev, D. G. Maloney, C. Andreadis, A. Sehgal, S. R. Solomon, N. Ghosh, C. Dehner, Y. Kim, K. Ogasawara, A. Kostic and T. Siddiqi, *Blood*, 2024, **143**, 404–416.
10 S. S. Neelapu, C. A. Jacobson, A. Ghobadi, D. B. Miklos, L. J. Lekakis, O. O. Oluwole, Y. Lin, I. Braunschweig, B. T. Hill, J. M. Timmerman, A. Deol, P. M. Reagan, P. Stiff, I. W. Flinn, U. Farooq, A. H. Goy, P. A. McSweeney, J. Munoz, T. Siddiqi, J. C. Chavez, A. F. Herrera, N. L. Bartlett, A. A. Bot, R. R. Shen, J. Dong, K. Singh, H. Miao, J. J. Kim, Y. Zheng and F. L. Locke, *Blood*, 2023, **141**, 2307–2315.
11 M. Wang, J. Munoz, A. Goy, F. L. Locke, C. A. Jacobson, B. T. Hill, J. M. Timmerman, H. Holmes, S. Jaglowski, I. W. Flinn, P. A. McSweeney, D. B. Miklos, J. M. Pagel, M.-J. Kersten, N. Milpied, H. Fung, M. S. Topp, R. Houot, A. Beitinjaneh, W. Peng, L. Zheng, J. M. Rossi, R. K. Jain, A. V. Rao and P. M. Reagan, *N. Engl. J. Med.*, 2020, **382**, 1331–1342.
12 K. V. Lepik and V. V. Markelov, *Cancers*, 2025, **17**, 317.
13 M. Ruella, F. Korell, P. Porazzi and M. V. Maus, *Nat. Rev. Drug Discovery*, 2023, **22**, 976–995.
14 P. Vormittag, R. Gunn, S. Ghorashian and F. S. Veraitch, *Curr. Opin. Biotechnol.*, 2018, **53**, 164–181.
15 S. Ghassemi, S. Nunez-Cruz, R. S. O'Connor, J. A. Fraietta, P. R. Patel, J. Scholler, D. M. Barrett, S. M. Lundh, M. M. Davis, F. Bedoya, C. Zhang, J. Leferovich, S. F. Lacey, B. L. Levine, S. A. Grupp, C. H. June, J. J. Melenhorst and M. C. Milone, *Cancer Immunol. Res.*, 2018, **6**, 1100–1109.
16 S. C. Jameson and D. Masopust, *Immunity*, 2018, **48**, 214–226.
17 L. Gattinoni, E. Lugli, Y. Ji, Z. Pos, C. M. Paulos, M. F. Quigley, J. R. Almeida, E. Gostick, Z. Yu, C. Carpenito, E. Wang, D. C. Douek, D. A. Price, C. H. June, F. M. Marincola, M. Roederer and N. P. Restifo, *Nat. Med.*, 2011, **17**, 1290–1297.
18 D. Meyran, J. J. Zhu, J. Butler, D. Tantalo, S. MacDonald, T. N. Nguyen, M. Wang, N. Thio, C. D'Souza, V. M. Qin, C. Slaney, A. Harrison, K. Sek, P. Petrone, K. Thia, L. Giuffrida, A. M. Scott, R. L. Terry, B. Tran, J. Desai, H. M. Prince, S. J. Harrison, P. A. Beavis, M. H. Kershaw, B. Solomon, P. G. Ekert, J. A. Trapani, P. K. Darcy and P. J. Neeson, *Sci. Transl. Med.*, 2023, **15**, eabk1900.
19 M. Ahmadi, N. Putnam, M. Dotson, D. Hayoun, J. Padilla, N. Fatima, P. Bhanap, G. Nonterah, X. de Mollerat du Jeu and Y. Ji, *Curr. Res. Transl. Med.*, 2025, **73**, 103489.
20 R. Stadel, N. Idippily, M. F. Giraudo, P. Caimi, K. Van Besien, J. Martin, J. Wu, C. Deng and D. Wald, *Blood*, 2023, **142**, 4848.
21 S. Ghassemi, J. S. Durgin, S. Nunez-Cruz, J. Patel, J. Leferovich, M. Pinzone, F. Shen, K. D. Cummins, G. Plesa, V. A. Cantu, S. Reddy, F. D. Bushman, S. I. Gill, U. O'Doherty, R. S. O'Connor and M. C. Milone, *Nat. Biomed. Eng.*, 2022, **6**, 118–128.
22 S. Arcangeli, C. Bove, C. Mezzanotte, B. Camisa, L. Falcone, F. Manfredi, E. Bezzecchi, R. El Khoury, R. Norata, F. Sanvito, M. Ponzoni, B. Greco, M. A. Moresco, M. G.

Carrabba, F. Ciceri, C. Bonini, A. Bondanza and M. Casucci, *J. Clin. Invest.*, 2022, **132**, e150807.

23 S. J. Schuster, M. R. Bishop, C. S. Tam, E. K. Waller, P. Borchmann, J. P. McGuirk, U. Jäger, S. Jaglowski, C. Andreadis, J. R. Westin, I. Fleury, V. Bachanova, S. R. Foley, P. J. Ho, S. Mielke, J. M. Magenau, H. Holte, S. Pantano, L. B. Pacaud, R. Awasthi, J. Chu, Ö. Anak, G. Salles and R. T. Maziarz, *N. Engl. J. Med.*, 2019, **380**, 45–56.

24 J. Yang, J. He, X. Zhang, J. Li, Z. Wang, Y. Zhang, L. Qiu, Q. Wu, Z. Sun, X. Ye, W. Yin, W. Cao, L. Shen, M. Sersch and P. Lu, *Blood Cancer J.*, 2022, **12**, 104.

25 P. A. Riedell, M. Kwon, I. W. Flinn, M. J. Dickinson, C. Solano, U. Jaeger, J. Briones, K. Kato, S. Fleming, E. Bachy, A. Rambaldi, L. O. Shune, N. N. Shah, D. Blaise, M. J. Frigault, A. Ramakrishnan, A. Yang, D. Pearson, A. Zia, E. Segura, A. Masood and P. Barba, *Blood*, 2024, **144**, 67.

26 C. A. Challener, *Pharm. Technol. Eur.*, 2019, **31**, 16–19.

27 F. Nina, G. Clive, V. Joseph, J. Pratik, K. Debbie, M. John, M. Alan, N. Josefina, P. Steve, P. Steven and others, *Cell Cult. Dish*, Port Wash. NY USA.

28 V. Sergeev, N. Emelyanova, V. Markelov and others, *Cell. Ther. Transplant.*, 2023, **12**, 2–51.

29 R. Tran, D. R. Myers, G. Denning, J. E. Shields, A. M. Lytle, H. Alrowais, Y. Qiu, Y. Sakurai, W. C. Li, O. Brand, J. M. Le Doux, H. T. Spencer, C. B. Doering and W. A. Lam, *Mol. Ther.*, 2017, **25**, 2372–2382.

30 W.-X. Sin, N. S. Jagannathan, D. B. L. Teo, F. Kairi, S. Y. Fong, J. H. L. Tan, D. Sandikin, K.-W. Cheung, Y. H. Luah, X. Wu, J. J. Raymond, F. L. W. I. Lim, Y. H. Lee, M. S.-F. Seng, S. Y. Soh, Q. Chen, R. J. Ram, L. Tucker-Kellogg and M. E. Birnbaum, *Nat. Biomed. Eng.*, 2024, **8**, 1571–1591.

31 K. V. Arabuli, E. Kopoleva, A. Akenoun, L. V. Mikhailova, E. Petrova, A. R. Muslimov, D. A. Senichkina, S. Tsymbal, A. I. Shakirova, A. I. Ignatiev, K. V. Lepik and M. V. Zyuzin, *Biomater. Adv.*, 2024, **161**, 213904.

32 N. Moore, J. R. Chevillet, L. J. Healey, C. McBrine, D. Doty, J. Santos, B. Teece, J. Truslow, V. Mott, P. Hsi, V. Tandon, J. T. Borenstein, J. Balestrini and K. Kotz, *Sci. Rep.*, 2019, **9**, 15101.

33 G. López-Cantillo, C. Urueña, B. A. Camacho and C. Ramírez-Segura, *Front. Immunol.*, 2022, **13**, 878209.

34 R. A. Gardner, O. Finney, C. Annesley, H. Brakke, C. Summers, K. Leger, M. Bleakley, C. Brown, S. Mgebroff, K. S. Kelly-Spratt, V. Hoglund, C. Lindgren, A. P. Oron, D. Li, S. R. Riddell, J. R. Park and M. C. Jensen, *Blood*, 2017, **129**, 3322–3331.

35 E. Galli, S. Bellesi, I. Pansini, G. Di Cesare, C. Iacovelli, R. Malafronte, E. Maiolo, P. Chiusolo, S. Sica, F. Sorà and S. Hohaus, *Br. J. Haematol.*, 2023, **203**, 564–570.